

2-dimensional hyperbolic medium for electrons and photons based on the array of tunnel-coupled graphene nanoribbons

Iurii Trushkov¹ and Ivan Iorsh¹

¹*National Research University of Information Technologies,
Mechanics and Optics (ITMO), St. Petersburg 197101, Russia*

We study the electronic band structure and optical conductivity of an array of tunnel-coupled array of graphene nanoribbons. We show that due to the coupling of electronic edge states for the zigzag nanoribbon structure, the Fermi surface can become a hyperbola similarly to the case of the layered metal-dielectric structures, where the hyperbolic isofrequency contours originate from the coupling of localized surface plasmon polaritons. Moreover, we show that for both types of the ribbon edge, the optical response of the structure can be characterized by a uniaxial conductivity tensor, having principal components of the different signs. Therefore, the tunnel-coupled nanoribbon array can be regarded as a tunable hyperbolic metasurface.

I. INTRODUCTION

Graphene is a two-dimensional carbon lattice that exhibits a wide range of unique electronic properties such as linear dispersion of charge carriers, Berry phase, and room-temperature quantum Hall effect^{1,2}. Beyond the purely electronic properties, graphene has attracted a lot of attention in the field of nanophotonics, since it is both transparent and exhibits strong light-matter interaction^{3,4}. Moreover, graphene supports the surface electromagnetic waves, analogous to surface plasmon polaritons in metallic and semiconductor films. The advantage of the graphene plasmon-polaritons over their metallic and semiconductor counterparts is that they can be efficiently controlled with the external gate voltage^{5,6}. The attractive plasmonic properties of graphene nanostructures led to the emerging of the field of graphene nanoplasmonics⁷.

One of the topics in graphene plasmonics is the study of graphene *metasurfaces*, the arrays of graphene nanoislands which may exhibit the optical properties which differ significantly from those of the two-dimensional graphene sheets^{8–11}. For example, it has been shown that a two-dimensional array of graphene nanoislands can play the role of a perfect absorber for electromagnetic waves¹². In the studies of graphene-based metasurfaces it is commonly assumed that the conductivity of individual graphene elements coincides with the conductivity of two-dimensional graphene. However, it is known from numerous studies that the graphene nanopatterning can substantially alter the electronic band structure of graphene^{13,14}. Specifically, in Ref.¹³ it was shown that one can open and efficiently control the width of the band gap by nanopatterning graphene. Altering the electronic band structure should lead to the modification of the AC conductivity and thus to the modification of the optical properties of the nanopatterned graphene. In Ref.¹⁵ it was theoretically shown that the quantum confinement effects start play the substantial role in the optical response of the patterned graphene if the characteristic size of the nanostructure elements becomes smaller than 10 nm. Technically, the introduction of the superlattice to the graphene sheet at these scales can be realized by ei-

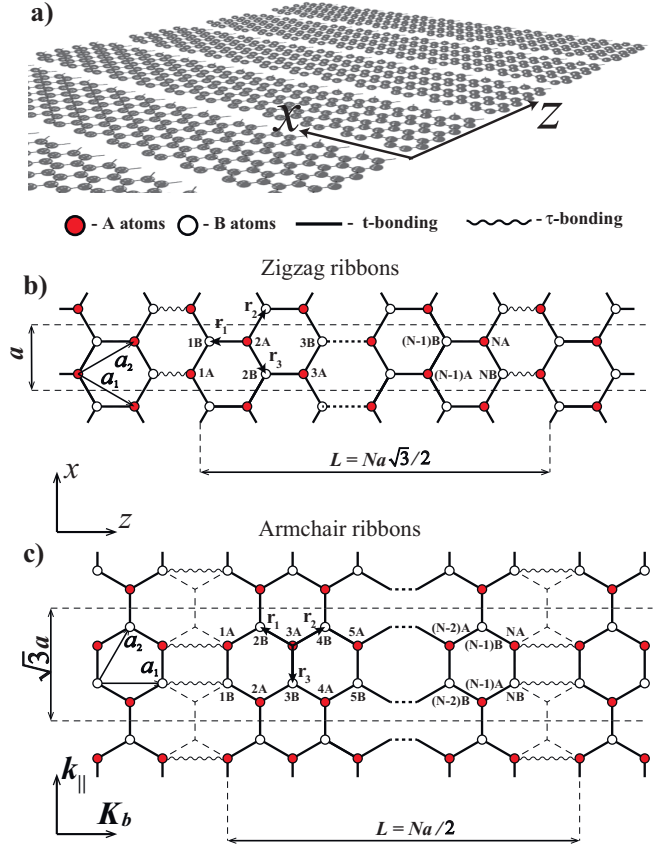


FIG. 1. (Color online) (a) Geometry of the structure (b,c) Structure the array of tunnel coupled array of zigzag (b) or armchair (c) graphene nanoribbons.

ther etching the graphene sheet¹⁶, introducing the periodic strain^{17–19} or by introducing the periodic gate voltage^{20,21}. Moreover, in Ref.²² the possibility of molecular assembly of the arrays of several-atoms-thick nanoribbons was shown.

In our work we are studying the structures shown in Fig.(1), which are essentially the arrays of tunnel-coupled graphene nanoribbons. We demonstrate that the optical properties of these structures can be tailored by engineering the electronic band structure, and that such a system

can be regarded as a uniaxial anisotropic medium both for electrons and plasmon-polaritons.

The remainder of the paper is organized as follows. In section II we show the results on the electronic band structure and Fermi surface topology of the arrays of zigzag and armchair graphene nanoribbons. Section III presents the results on the conductivity spectra obtained with the Kubo formula. The conclusion of the paper is given in section IV. Finally, appendices A and B provide the detailed formalism for the calculation of the band structure and the conductivity, respectively.

II. BAND STRUCTURE CALCULATION

For both types of the ribbons edge the Hamiltonian can be written as²³:

$$\begin{aligned} \hat{H} = & -t \sum_{\text{nearest}} (\hat{a}_\alpha^\dagger \hat{b}_\beta + \hat{b}_\beta^\dagger \hat{a}_\alpha) - t' \sum_{\substack{\text{next} \\ \text{nearest}}} (\hat{a}_\alpha^\dagger \hat{a}_\beta + \hat{b}_\alpha^\dagger \hat{b}_\beta) - \\ & -\tau \sum_{\substack{\text{inter-} \\ \text{ribbon}}} (\hat{a}_\alpha^\dagger \hat{b}_\beta + \hat{b}_\beta^\dagger \hat{a}_\alpha), \end{aligned} \quad (1)$$

where the first term corresponds to the hopping of the electron between the nearest atoms with the characteristic hopping energy $t = 2.8$ eV, the second term to the next-nearest hopping with $t' = 0.2$ eV, and the last term corresponds to the tunneling between the nearest ribbons with the tunneling energy τ which can be varied (see Fig.1). Generally, τ should decrease exponentially with distance between the neighbouring ribbons \tilde{a} $\tau \approx t \exp(-2(\tilde{a} - a)/a)$ ²⁴, where a is the interatomic distance. We note that as \tilde{a} goes to infinity, the band structure and the conductivity should reduce to those of an individual nanoribbon. In the opposite limit $\tilde{a} = a$, the considered structure can either converge to the conventional 2d graphene case as in Fig.1(c) or result in a more complicated structure different from the two-dimensional graphene as in Fig.1(c). In our calculations we have used $\tilde{a} = \sqrt{3}a$ which corresponds to $\tau = t'$.

Indices $[\alpha, \beta]$ in the Eq. (1) each consist of three integers: the first one i is the number of the atom in the unit cell. The unit cells for the case of armchair and zigzag ribbons are shown with dashed lines in Figs. 1(b,c). Each unit cell contains N atoms of each sublattice. The remaining two indices (m, n) correspond to the position of the unit cell in the directions of K_b and k , respectively (cf. Figs 1(b,c) for further details). We then introduce Fourier transform of the annihilation and creation operators $a_\alpha, a_\alpha^\dagger$:

$$\begin{aligned} a_{i,m,n} &= \frac{1}{N_c^{1/2}} \sum_{k, K_b} a_i(k, K_b) e^{-i(K_b m L + k n a)}, \\ a_{i,m,n}^\dagger &= \frac{1}{N_c^{1/2}} \sum_{k, K_b} a_i^\dagger(k, K_b) e^{i(K_b m L + k n a)} \end{aligned} \quad (2)$$

where N_c is the number of unit cells. The expressions for the operators b are identical. The wave functions of the

structure are the linear combinations of the single atom eigenfunctions:

$$\phi(k, K_b) = \sum_{i=1, N} \left[\mathcal{A}_i a_i^\dagger(k, K_b) |0\rangle + \mathcal{B}_i b_i^\dagger(k, K_b) |0\rangle \right], \quad (3)$$

and thus can be represented as a $2N$ vector of the expansion coefficients \mathcal{A}, \mathcal{B} :

$$\phi = (\mathcal{A}_1 \dots \mathcal{A}_N, \mathcal{B}_1 \dots \mathcal{B}_N)^T. \quad (4)$$

If we substitute the expressions (2) to the Hamiltonian (1) we obtain $H = \sum_{k, K_b} H(k, K_b)$, where $H(k, K_b)$ can be represented as a $2N \times 2N$ matrix in the basis of the single atom eigenfunctions:

$$H = \begin{pmatrix} H_{AA} & H_{AB} \\ H_{BA} & H_{BB} \end{pmatrix}. \quad (5)$$

Explicit form of the matrix depends on the type of the ribbon edge and is presented in appendix A for both types of the edge, here we just note that due to the requirement of Hermiticity the condition $H_{BA} = H_{AB}^\dagger$ holds.

The problem is then reduced to the eigenvalue problem for a $2N \times 2N$ matrix $H(k, K_b)\phi = \epsilon(k, K_b)\phi$, which has been solved numerically in order to obtain the band structures and Fermi surfaces. For the case of zigzag ribbons $N = 10$ and for the case of armchair ribbons $N = 11$. The results are presented in Figs.2,3 We first consider the zigzag edge case shown in Fig.2. We first note, that due to the inclusion of the second nearest neighbours hopping, the electron-hole symmetry is broken and the electron and hole bands touch at the nonzero energy²⁵. It can be seen that the individual branches of the single ribbon band diagram evolve to the bands. Moreover, the degeneracy of the two edge states is lifted and we observe two distinct bands formed by the tunnel coupled edge states. These bands resemble the plasmonic bands existing in the layered metal-dielectric structures²⁶ and originating from the photon tunneling between individual surface plasmon polaritons propagating along the metal-dielectric interfaces. It is these plasmonic bands that form the hyperbolic isofrequency contours and make the layered metal dielectric structures the most conventional realization of hyperbolic medium²⁷. As can be seen in Fig.2(b), where the energy contour plots are presented, the similar situation takes place for the electrons in coupled zigzag ribbons. At the energy where the electron and hole bands touch (equal to $3t' \approx 0.6$ eV) the contour plots reduce to single points at the touching position. Then, as we shift to the area where the band formed by the edge states exists, we can observe the hyperbolic-like isofrequency contours. Thus, if the chemical potential is tuned such that the Fermi energy falls to the narrow region of these bands, the electrons at the Fermi surface would propagate in the effective hyperbolic media. We also note that at certain energies the Fermi contour reduces to parallel lines, and the two-dimensional structure effectively behaves as a one dimensional. As it is known²⁸, in the

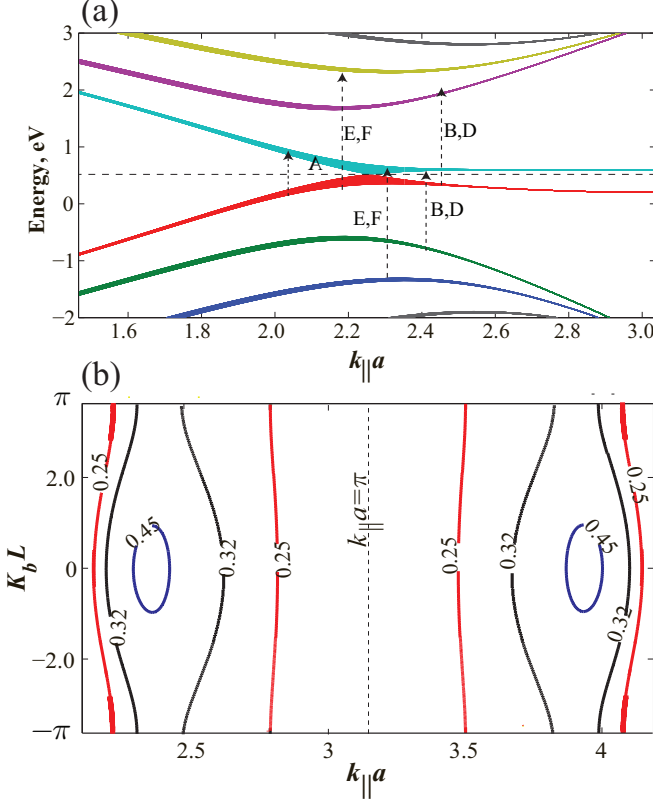


FIG. 2. (Color online) Electronic band structure of the array of tunnel coupled zigzag nanoribbons. (b) Contour plots of the Fermi surfaces of the structure. The numbers at the curves define the corresponding electron energy.

vicinity of such points the electron-electron interactions are substantially modified and the inclusion of the Hubbard repulsion to our tight-binding model is the subject of the future work. The advantage of the graphene-based structures is that the Fermi level can be fine-tuned with the external gate voltage, such that it falls to the region characterized by the hyperbolic isofrequency contour.

The band diagram and the Fermi surface contour plots for the case of an armchair ribbons are shown in Fig.3. For the case of armchair ribbon, the Dirac cones exist only if the number of atoms in the unit cell $N = 3m + 2$, where m is an integer²⁵. In the considered structure $N = 11$ and thus the Dirac cones are preserved. It can be seen that coupling leads to the overlap of the electron and hole bands, and thus as can be seen in Fig.3(b) at certain Fermi energies, the Fermi surface contains both electron and hole pockets.

We now move to the calculation of the AC conductivity of the considered structures.

III. CONDUCTIVITY TENSOR.

When the eigenvalues and eigenvectors are obtained, it is straightforward to compute the AC conductivity tensor of the structure using the Kubo formalism. The conduc-

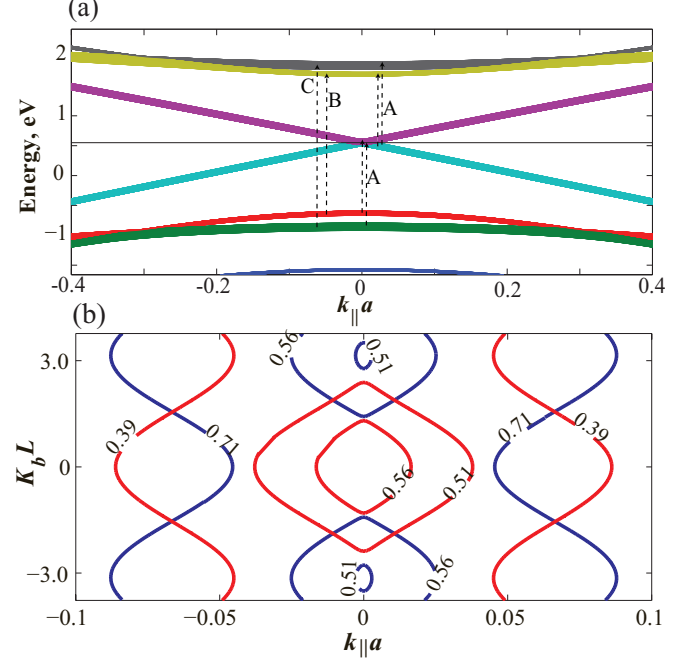


FIG. 3. (Color online) Electronic band structure of the array of tunnel coupled armchair nanoribbons. (b) Contour plots of the Fermi surfaces of the structure. Blue (red) curves correspond to electron (hole) branches. The numbers on the curves define the corresponding electron energy.

tivity tensor is given by²⁹

$$\sigma_{\alpha\alpha} = \frac{\hbar}{iS} \sum_{s',s} \sum_{n,m} \frac{\left(f[\varepsilon_m^{s'}] - f[\varepsilon_n^s] \right) \left| \langle \phi_m^{s'} | -ev_\alpha | \phi_n^s \rangle \right|^2}{(\varepsilon_m^{s'} - \varepsilon_n^s)(\varepsilon_m^{s'} - \varepsilon_n^s + \hbar\omega + i\delta)} \quad (6)$$

The velocity operator \mathbf{v} is defined through $-e\mathbf{v}/c = \partial H(\mathbf{A})/\partial \mathbf{A}$, where $H(\mathbf{A})$ is derived from the tight-binding model via Peierls substitution:

$$t_{\mathbf{R},\mathbf{R}'} \rightarrow t_{\mathbf{R},\mathbf{R}'} e^{\frac{ie}{\hbar c} \int_{\mathbf{R}}^{\mathbf{R}'} \mathbf{A} d\mathbf{r}} = t_{\mathbf{R},\mathbf{R}'} e^{\frac{ie}{\hbar c} (\mathbf{R}' - \mathbf{R}) \mathbf{A}}. \quad (7)$$

The latter equality is made within the approximation that the vector potential is constant at the scale of single unit cell. The velocity operator then can be presented as an $2N \times 2N$ matrix of the form:

$$-e\mathbf{v} = -e \begin{pmatrix} \mathbf{v}_{AA} & \mathbf{v}_{AB} \\ \mathbf{v}_{BA} & \mathbf{v}_{BB} \end{pmatrix}. \quad (8)$$

Due to the requirement of the hermiticity of the velocity operator, we set $\mathbf{v}_{AB} = \mathbf{v}_{BA}^\dagger$ and within the nearest neighbour approximation $\mathbf{v}_{AA} = \mathbf{v}_{BB} = 0$. The explicit form of \mathbf{v}_{AB} depends on the type of the edge and is presented in the appendix B. The results are shown in Figs.4(a,b). The temperature was set to 300K and the chemical potential was equal to $3t'$. The conductivity is normalized to the bare graphene conductivity $\sigma_0 = e^2/\hbar$. For the case of zigzag ribbons, we observe the strong ab-

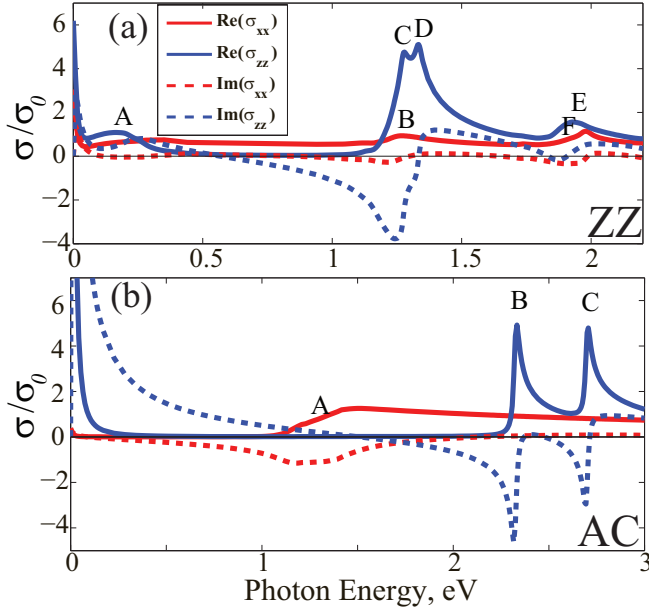


FIG. 4. (Color online) Real and imaginary parts of the principal components of the conductivity tensor for the case of zigzag (a) and armchair (b) ribbon edge. Letters in (a) and (b) correspond to the transitions shown in Fig.2(a) and Fig.3(a) respectively.

sorption for the field polarized along the ribbons. This effect is due to the presence of the edge states and is also present in the conductivity spectra of individual zigzag ribbons³⁰. However, due to the lift of degeneracy between the edge states, an additional absorption channel between the two edge states bands appears, which results in the broad resonance of the absorption for the transverse-polarized electric field, depicted with letter A in Fig.4(a). In the low frequency region, the conductivity has the Drude-like shape for both electric field polarizations. In the higher frequency region the conductivity is determined by the interband transitions shown in Fig.2(a). In the certain frequency region the absorption is suppressed, and the imaginary parts of the conductivity tensor components have opposite signs.

We should also note, that the obtained conductivity tensors are nonlocal, i.e. the conductivity depends on the in-plane momenta of the electromagnetic wave. In Fig. 5 the real part of the conductivity of both zigzag and armchair ribbons is presented for different values of $K_b D$ and compared to the conductivity of two-dimensional graphene. The substantial modification of the real part of the conductivity is observed due to the opening of new absorption channels via the indirect interband transitions.

IV. CONCLUSION AND OUTLOOK.

In this paper, we have analyzed the electronic band structure and conductivity spectrum of two-dimensional arrays of tunnel-coupled arrays of graphene nanoribbons.

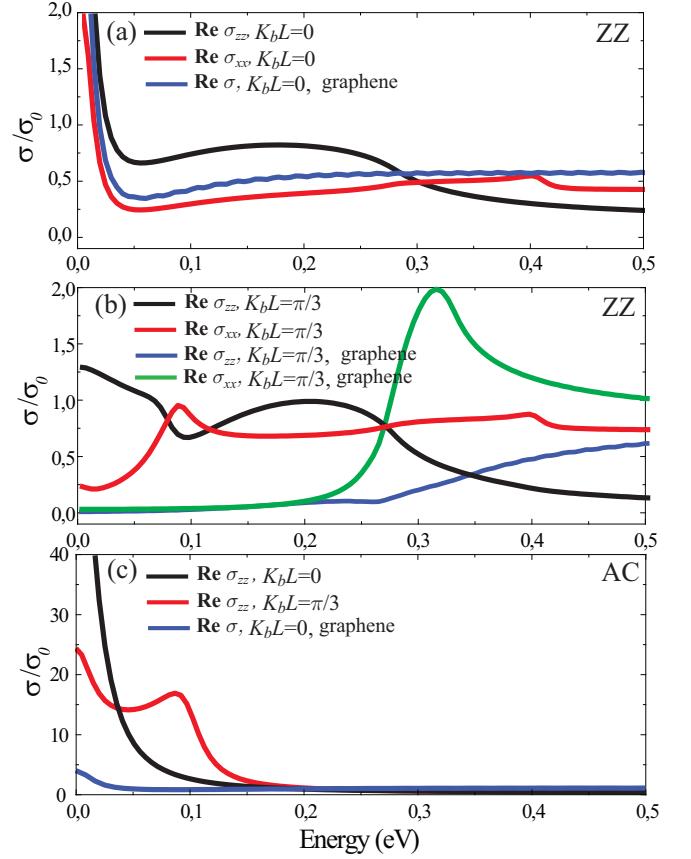


FIG. 5. (Color online) Conductivity spectrum for the zigzag (a,b) and armchair (c) ribbons for different values of $K_b D$. The conductivity of two-dimensional graphene is shown for comparison.

We have shown that both depend drastically on the type of the ribbon edges. Namely, for the case of zigzag edges the coupling of the electronic edge states lifts the degeneracy between the symmetric and antisymmetric electronic eigenmode formed by the edge states. Moreover, each of the individual modes evolves to a narrow band, defined by the hyperbolic isofrequency surfaces. We have thus demonstrated the simple yet interesting analogy between the considered structures and multilayered metal-dielectric metamaterials, where the hyperbolic isofrequency surface for the electromagnetic field originates from the coupling between individual surface-plasmon polariton modes. For the case of armchair ribbons, we have shown that the coupling leads to the overlap of electron and hole bands, resulting into the formation of the hole and electron pockets in the Fermi surface of these structures in the certain doping range.

Furthermore, we have shown that these structures can be regarded as metasurfaces for the electromagnetic waves in the optical to mid-IR frequency range³¹. Specifically, we have demonstrated that both types of the structures are characterized by different signs of imaginary part of conductivity tensor components together with small levels in some frequency ranges. Recently, a phenomenological study of the electromagnetic spectrum

of such metasurfaces has been performed, showing that these structures can support a special type of Dyakonov-like hybrid surface electromagnetic waves³².

The modification of the electronic band structures as well as electronic eigenfunction profiles in the nanostructured graphene should lead to the substantial modification of the electron-electron interactions. Self-consistent calculation of the Coulomb self-energy as well as interactions-induced modification of the AC conductivity is the subject of future work. Availability to control the optical response of the graphene metasurfaces via the modification of the electronic band structure through the quantum confinement makes these structure a perspective platform for the novel optical to IR optoelectronic devices.

Appendix A: Band structure calculation

Below is presented the explicit form of the Hamiltonian from Eq. (5) for both types of the ribbons edge.

Zigzag edge:

$$H_{AB} = -t \cdot \begin{pmatrix} \kappa & 0 & 0 & \dots & 0 & \frac{\tau}{t} e^{iK_b L} \\ 1 & \kappa^* & 0 & \dots & 0 & 0 \\ 0 & 1 & \kappa & \dots & 0 & 0 \\ \vdots & \vdots & \vdots & \ddots & \vdots & \vdots \\ 0 & 0 & 0 & \dots & \kappa & 0 \\ 0 & 0 & 0 & \dots & 1 & \kappa^* \end{pmatrix}, \quad (A1)$$

$$H_{AA} = -2t' \cdot \begin{pmatrix} \cos ka & \frac{\kappa}{2} & 0 & \dots & 0 \\ \frac{\kappa^*}{2} & \cos ka & \frac{\kappa^*}{2} & \dots & 0 \\ 0 & \frac{\kappa}{2} & \cos ka & \dots & 0 \\ \vdots & \vdots & \vdots & \ddots & \vdots \\ 0 & 0 & 0 & \dots & \frac{\kappa}{2} \\ 0 & 0 & 0 & \dots & \cos ka \end{pmatrix}, \quad (A2)$$

where $\kappa = 1 + e^{ika}$, $L = Na\sqrt{3}/2$, $H_{BA} = H_{AB}^\dagger$, $H_{BB} = H_{AA}^*$.

Armchair edge:

$$H_{AB} = -t \cdot \begin{pmatrix} 1 & 1 & \dots & 0 & 0 \\ 1 & e^{ik\sqrt{3}a} & \dots & 0 & 0 \\ \vdots & \vdots & \ddots & \vdots & \vdots \\ 0 & 0 & \dots & e^{ik\sqrt{3}a} & 1 \\ 0 & 0 & \dots & 1 & 1 \end{pmatrix}, \quad (A3)$$

$$H_{AA} = -t' \cdot \begin{pmatrix} 0 & \kappa^* & 1 & \dots & 0 & 0 & \frac{\tau}{t'} e^{iK_b L} \\ \kappa & 0 & \kappa & \dots & 0 & 0 & 0 \\ 1 & \kappa^* & \kappa^* & \dots & 0 & 0 & 0 \\ 0 & 1 & \kappa & \dots & 0 & 0 & 0 \\ \vdots & \vdots & \vdots & \ddots & \vdots & \vdots & \vdots \\ 0 & 0 & 0 & \dots & 0 & \kappa^* & 1 \\ 0 & 0 & 0 & \dots & \kappa & 0 & \kappa \\ \frac{\tau}{t'} e^{-iK_b L} & 0 & 0 & \dots & 1 & \kappa^* & 0 \end{pmatrix}, \quad (A4)$$

$$H_{BB} = -t' \cdot \begin{pmatrix} 0 & \kappa & 1 & \dots & 0 & 0 & \frac{\tau}{t'} e^{iK_b L} \\ \kappa^* & 0 & \kappa^* & \dots & 0 & 0 & 0 \\ 1 & \kappa & \kappa & \dots & 0 & 0 & 0 \\ 0 & 1 & \kappa^* & \dots & 0 & 0 & 0 \\ \vdots & \vdots & \vdots & \ddots & \vdots & \vdots & \vdots \\ 0 & 0 & 0 & \dots & 0 & \kappa & 1 \\ 0 & 0 & 0 & \dots & \kappa^* & 0 & \kappa^* \\ \frac{\tau}{t'} e^{-iK_b L} & 0 & 0 & \dots & 1 & \kappa & 0 \end{pmatrix}, \quad (A5)$$

where $\kappa = 1 + e^{ika\sqrt{3}}$, $L = Na/2$, $H_{BA} = H_{AB}^\dagger$.

Appendix B: Calculation of the AC conductivity

The expression for the conductivity operator for the case of zigzag edge is given by:

$$-e\mathbf{v}_{AB} = -\frac{ie}{\hbar} t \cdot \begin{pmatrix} \mathbf{r}_2 + \mathbf{r}_3 e^{ika} & 0 & 0 & \dots & 0 & 0 \\ \mathbf{r}_1 & \mathbf{r}_3 + \mathbf{r}_2 e^{-ika} & 0 & \dots & 0 & 0 \\ 0 & \mathbf{r}_1 & \mathbf{r}_2 + \mathbf{r}_3 e^{ika} & \dots & 0 & 0 \\ \vdots & \vdots & \vdots & \ddots & \vdots & \vdots \\ 0 & 0 & 0 & \dots & \mathbf{r}_2 + \mathbf{r}_3 e^{ika} & 0 \\ 0 & 0 & 0 & \dots & \mathbf{r}_1 & \mathbf{r}_3 + \mathbf{r}_2 e^{-ika} \end{pmatrix}, \quad (B1)$$

with $\mathbf{r}_1 = a/\sqrt{3}(-1, 0)$; $\mathbf{r}_2 = a/\sqrt{3}(1/2, \sqrt{3}/2)$; $\mathbf{r}_3 = a/\sqrt{3}(1/2, -\sqrt{3}/2)$, and for the case of armchair edge is

given by

$$-e\mathbf{v}_{AB} = -\frac{ie}{\hbar} t \cdot \begin{pmatrix} \mathbf{r}_3 & \mathbf{r}_2 & 0 & \dots & 0 & 0 \\ \mathbf{r}_1 & \mathbf{r}_3 e^{ik\sqrt{3}a} & \mathbf{r}_2 & \dots & 0 & 0 \\ 0 & \mathbf{r}_1 & \mathbf{r}_3 & \dots & 0 & 0 \\ \vdots & \vdots & \vdots & \ddots & \vdots & \vdots \\ 0 & 0 & 0 & \dots & \mathbf{r}_3 e^{ik\sqrt{3}a} & \mathbf{r}_2 \\ 0 & 0 & 0 & \dots & \mathbf{r}_1 & \mathbf{r}_3 \end{pmatrix},$$

with $\mathbf{r}_1 = a/\sqrt{3}(-\sqrt{3}/2, 1/2)$; $\mathbf{r}_2 = a/\sqrt{3}(\sqrt{3}/2, 1/2)$; $\mathbf{r}_3 = a/\sqrt{3}(0, -1)$.

-
- ¹ R.R. Nair, P. Blake, A.N. Grigorenko, K.S. Novoselov, T.J. Booth, T. Stauber, N.M.R. Peres, and A.K. Geim, *Science* **320**, 1308 (2008).
 - ² Q. Bao and K.P. Loh, *ACS Nano* **6**, 3677 (2012).
 - ³ F. Bonaccorso, Z. Sun, T. Hasan, and A.C. Ferrari, *Nature Photonics*, **4**, 611, 2010.
 - ⁴ P. Avouris, *Nano Letters*, **10**, 4285, 2010.
 - ⁵ J. Chen, M. Badioli, P. Alonso-Gonzales, S. Thongrattanasiri, F. Huth, J. Osmond, M. Spasenovic, A. Centeno, A. Pesquera, P. Godignon, A.Z. Elorza, N. Camara, F. J.G. de Abajo, R. Hillenbrand, and F.H.L. Koppens, *Nature (London)* **487**, 77 (2012).
 - ⁶ Z. Fei, A. S. Rodin, G.O. Andreev, W. Bao, A.S. McLeod, M. Wagner, L.M. Zhang, Z. Zhao, G. Dominguez, M. Thiemens, M.M. Fogler, A.H. Castro-Neto, C.N. Lau, F. Keilmann, and D.N. Basov, *Nature (London)* **487**, 82 (2012).
 - ⁷ A.N. Grigorenko, M. Polini, K.S. Novoselov, *Nature Photonics* **6**, 749758, 2012.
 - ⁸ A. Fallahi and Ju. Perruisseau-Carrier, *Phys. Rev. B* **86**, 195408, 2012.
 - ⁹ H. Cheng, S. Chen, P. Yu, X. Duan, B. Xie and J. Tian, *Applied Physics Letters*, **103**, 203112, 2013.
 - ¹⁰ P. Chen, J. Soric, Y.R. Padooru, H.M. Bernety, A.B. Yakovlev and A. Alu, *New Journal of Physics*, **15** 123029, 2013.
 - ¹¹ A. Vakil, N. Engheta, *Science*, **232**, 1291, 2011.
 - ¹² S. Thongrattanasiri, F.H.L. Koppens, and F. Javier Garca de Abajo, *Physical Review Letters*, **108**, 047401, 2012.
 - ¹³ M. Dvorak, W. Oswald and Z. Wu, *Scientific report*, **3**, 2289, 2013.
 - ¹⁴ S.R. Power and A.P. Jauho, *Physical Review B*, **90**, 115408, 2014.
 - ¹⁵ S. Thongrattanasiri, A. Manjavacas, F. Javier Garca de Abajo, *ACS Nano*, **6**, 1766, 2012.
 - ¹⁶ X. Wang, H. Dai, *Nature Chemistry*, **2**, 661, 2010.
 - ¹⁷ W. Bao, F. Miao, Z. Chen, H. Zhang, W. Jang, C. Dames, C.N. Lau, *Nature Nanotechnology*,
 - ¹⁸ W. Bao, F. Miao, Z. Chen, H. Zhang, W. Jang, C. Dames, C.N. Lau, L. Tapaszt, T. Dumitrica, S.J. Kim, P. Nems-Incze, C. Hwang, L.P. Biro, *Nature Physics*, **8**, 739, 2012.
 - ¹⁹ C. Lin, X. Huang, F. Ke, C. Jin, N. Tong, X. Yin, L. Gan, X. Guo, R. Zhao, W. Yang, E. Wang, and Z. Hu, *Physical Review B*, **89**, 085416, 2014.
 - ²⁰ C.-H. Park, L. Yang, Y.W. Son, M.L. Cohen, S.H. Louie, *Nature Physics*, **4**, 213, 2008.
 - ²¹ M. Barbier, P. Vasilopoulos, F.M. Peeters, *Physical Review B*, **81**, 075438, 2010.
 - ²² Y.-C. Chen, T. Cao, C. Chen, Z. Pedramrazi, D. Haberer, D.G. de Oteyza, F.R. Fischer, S.G. Louie, and M.F. Crommi, *Nature Nanotechnology*, doi:10.1038/nnano.2014.307 (published online), 2015.
 - ²³ M. Katsnelson, *Graphene: carbon in two dimensions*, Cambridge University Press, 2012.
 - ²⁴ V.L. Katkov, V.A. Osipov, *JETP Letter*, **98**, 689, 2013.
 - ²⁵ A.H. Castro-Neto, F. Guinea, N.M.R. Peres, K.S. Novoselov, A.K. Geim, *Reviews of Modern Physics*, **81**,110, 2009.
 - ²⁶ A. A. Orlov, P.M. Voroshilov, P.A. Belov, and Yu.S. Kivshar, *Phys. Rev. B*, **84**,045424, 2011.
 - ²⁷ A.N. Poddubny, I.Iorsh, P.A. Belov, Yu.S. Kivshar, *Nature Photonics*, **7**, 948, 2013.
 - ²⁸ D.M. Newns, H.R. Krishnamurthy, P. Pattnaik, C.Tsuei, C.L. Kane, *Phys. Rev. Letters*, **69**, 1264, 1992.
 - ²⁹ H. Bruuc, K. Flensberg, *Many-Body Quantum Theory in Condensed Matter Physics*, Oxford University Press, 2001.
 - ³⁰ K. Sasaki, K. Kato, Y. Tokura, K. Oguri, and T. Sogawa, *Physical Review B*, **84**, 085458, 2011.
 - ³¹ A.V. Kildishev, A. Boltasseva, V. M. Shalaev, *Science*, **339**, 6125, 2013.
 - ³² O. Yermakov, A. Ovcharenko, A. Bogdanov, I. Iorsh, Yu. S. Kivshar, arXiv:1502.07468 [physics.optics], 2015.